THE JOURNAL OF PHYSICAL CHEMISTRY B

pubs.acs.org/JPCB Article

Conformational Differences Are Observed for the Active and Inactive Forms of Pinholin S^{21} Using DEER Spectroscopy

Tanbir Ahammad, Daniel L. Drew, Jr., Indra D. Sahu, Rasal H. Khan, Brandon J. Butcher, Rachel A. Serafin, Alberto P. Galende, Robert M. McCarrick, and Gary A. Lorigan*

Cite This: *J. Phys. Chem. B* 2020, 124, 11396−11405 Read Online

ACCESS | Metrics & More | Article Recommendations | Supporting Information

ABSTRACT: Bacteriophages have evolved with an efficient host cell lysis mechanism to terminate the infection cycle and release the new progeny virions at the optimum time, allowing adaptation with the changing host and environment. Among the lytic proteins, holin controls the first and rate-limiting step of host cell lysis by permeabilizing the inner membrane at an allele-specific time known as "holin triggering". Pinholin S^{21} is a prototype holin of phage Φ21 which makes many nanoscale holes and destroys the proton motive force, which in turn activates the signal anchor release (SAR) endolysin system to degrade the peptidoglycan layer of the host cell and destruction of the outer membrane by the spanin complex. Like many others, phage Φ21 has two holin proteins: active pinholin and antipinholin. The antipinholin form differs only by three extra amino acids at the N-terminus; however, it has a different structural topology and conformation with respect to the membrane. Predefined combinations of active pinholin and antipinholin fine-tune the lysis timing through structural dynamics and conformational changes. Previously, the dynamics and topology of active pinholin and antipinholin were investigated (Ahammad et al. *JPCB* **2019, 2020**) using continuous wave electron paramagnetic resonance (CW-EPR) spectroscopy. However, detailed structural studies and direct comparison of these two forms of pinholin S^{21} are absent in the literature. In this study, the structural topology and conformations of active pinholin ($S^{21}68$) and inactive antipinholin ($S^{21}68_{IRS}$) in DMPC (1,2-dimyristoyl-*sn*-glycero-3-phosphocholine) proteoliposomes were investigated using the four-pulse double electron−electron resonance (DEER) EPR spectroscopic technique to measure distances between transmembrane domains 1 and 2 (TMD1 and TMD2). Five sets of interlabel distances were measured via DEER spectroscopy for both the active and inactive forms of pinholin S^{21}. Structural models of the active pinholin and inactive antipinholin forms in DMPC proteoliposomes were obtained using the experimental DEER distances coupled with the simulated annealing software package Xplor-NIH. TMD2 of $S^{21}68$ remains in the lipid bilayer, and TMD1 is partially externalized from the bilayer with some residues located on the surface. However, both TMDs remain incorporated in the lipid bilayer for the inactive $S^{21}68_{IRS}$ form. This study demonstrates, for the first time, clear structural topology and conformational differences between the two forms of pinholin S^{21}. This work will pave the way for further studies of other holin systems using the DEER spectroscopic technique and will give structural insight into these biological clocks in molecular detail.

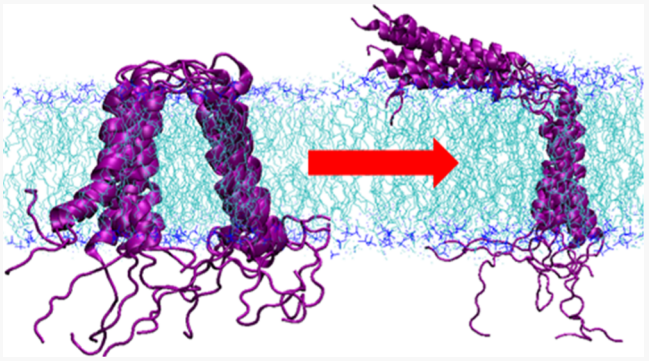

INTRODUCTION

Phage therapy has been revived in the current era of antimicrobial resistance to combat multidrug-resistant bacteria.[1−6] Phages and their bacteriolytic gene cassettes can serve as effective biocontrol agents for food safety and preservation.[7−9] The holin−endolysin system at the center of these bacteriolytic gene cassettes has potential therapeutic and pathophysiological application in higher animals.[1−5,10−13] It is a prerequisite to understand the bacteriophage life cycle and its lytic system for the judicious use of bacteriophages. Phages devised a robust lytic system to control the length of the infection cycle in response to the changing environment and host.[14] Most large, dsDNA bacteriophages evolved with an efficient host lysis system instrumental to lyse host cells at an optimum time. At least three proteins, the holin, endolysin, and spanin, are needed to lyse the Gram-negative bacterial cells.[15−18] Spanins degrade the outer membrane, whereas endolysin is the key component of this lysis machinery, which degrades the peptidoglycan layer within a few seconds of reaching the target site.[14,15,19] However, holin is the molecular clock responsible for the precise timing of host cell

Received: October 6, 2020
Revised: November 25, 2020
Published: December 8, 2020

https://dx.doi.org/10.1021/acs.jpcb.0c09081
J. Phys. Chem. B 2020, 124, 11396−11405

lysis.[15,20−24] Holin triggers at an allele-specific time and concentration to make micron-scale holes.[21,25−29] These holes are large enough to allow the fully folded functional endolysin to cross the inner membrane to reach the peptidoglycan layer.[14,30] More recently, a prototype holin system was discovered in some phages, which makes smaller holes comparable to the canonical holin, and denoted as pinholin.[31,32] Pinholins are coupled with the signal anchor release (SAR) endolysin system which maintains a membrane-tethered inactive conformation during the vegetative phase of the phage infection cycle.[31] Like canonical holin, pinholin triggers at an allele-specific time and concentration to permeabilize the cytoplasmic membrane. However, in contrast to the canonical holin, pinholin makes a large number of nanoscale holes and destroys the proton motive force which accelerates the release and activation of SAR endolysin to degrade the peptidoglycan layer.[31,33]

Pinholin S^{21} is a class-II holin, encoded by the S^{21} gene of phage Φ21.[18,34] S^{21} is a dual-start motif gene; it encodes two holin proteins, a lysis effector (pinholin $S^{21}68$) and lysis inhibitor (antipinholin $S^{21}71$).[34] Both of these proteins have two transmembrane domains (TMDs), which initially remain incorporated in the bacterial inner cytoplasmic membrane (ICM) and accumulate harmlessly as inactive dimers.[32,35] However, TMD1 of $S^{21}68$ externalizes very quickly from the ICM, which is the prerequisite for the active dimer and its subsequent oligomerization for pinhole formation. Conversely, TMD1 of $S^{21}71$ externalizes slowly, which in turn delays the initial oligomerization and pinhole formation.[32] A proper combination of active pinholin and antipinholin gives precise timing of host cell lysis.[36]

The functional difference between pinholin and antipinholin has been attributed to the presence of an extra positively charged amino acid in $S^{21}71$.[32,34] However, after the initial delay of externalization, TMD1 of $S^{21}71$ is exported to the periplasm and achieves a similar topology to $S^{21}68$, which makes it inconvenient for the topological study of antipinholin using conventional spectroscopic techniques. Instead of $S^{21}71$, Young's group reported a structural analogue of antipinholin by adding five extra amino acids (RYIRS) after the Met at the N terminal of active pinholin, referred to as $S^{21}68_{IRS}$.[32,37] This "RYIRS" tag prevents the externalization of TMD1 from the lipid bilayer and is reported as a dominant inhibitor of pinholin, which makes it a more feasible structural analogue of antipinholin S^{21} for the structural dynamics and topological study using biophysical techniques.[32,35,37]

It is well accepted that a protein's stability and functions are dictated by its structural topology and dynamic properties.[38−42] Hence, it is vital to know the structural details and topological differences between pinholin and antipinholin to understand the structure−activity relationship of this molecular clock mechanism. Pinholin systems were extensively studied by the Young lab using biomolecular and functional techniques.[31,32,34−37,43] However, the structural dynamics, topology, and conformational changes of pinholin have not been extensively investigated using biophysical techniques. There are no detailed structural studies of this system using conventional biophysical techniques such as X-ray crystallography, Cryo-EM, and NMR spectroscopy because of the fact that the study of membrane proteins in the presence of lipid vesicles is challenging using these techniques.[44−47] CD experiments have indicated that both forms of pinholin are mostly α-helical.[48−50] Electron paramagnetic resonance (EPR) spectroscopy is a powerful biophysical technique to study the membrane protein structure and dynamics in lipid environments with high sensitivity and without any size limitations.[38,51−61] Recently, the Lorigan lab reported a tentative model of pinholin S^{21} using CW-EPR power saturation and solid-state (SS)-NMR spectroscopic techniques.[48,49,62] It was reported that TMD1 and TMD2 of inactive antipinholin were incorporated into the lipid bilayer.[49] However, TMD1 was externalized from the lipid bilayer and remained on the surface of the lipid bilayer for active pinholin.[48] However, higher quality structural data are needed to clearly describe the conformation and topology of the different forms of pinholin.[33,48,49,62]

To investigate the membrane topology and structural conformational differences of pinholin ($S^{21}68$) and antipinholin ($S^{21}68_{IRS}$) in a lipid bilayer, four-pulse double electron−electron resonance (DEER) spectroscopy was used, which can probe the distance between two EPR spin labels strategically placed in TMD1 and TMD2. DEER spectroscopy coupled with site-directed spin labeling (SDSL) is a powerful biophysical tool for long-range distance (20−70 Å) measurements in biomolecules.[51,63−68] For this study, full-length pinholin and antipinholin were synthesized using Fmoc solid-phase peptide synthesis (Fmoc-SPPS). A nitroxide spin label, MTSL (S-(1-oxyl-2,2,5,5-tetramethyl-2,5-dihydro-1H-pyrrol-3-yl) methyl ethanesulfonothioate), was attached by SDSL to make an EPR active pinholin S^{21} construct.[48,69] DEER measurements were carried out on several dual spin-labeled active pinholin ($S^{21}68$) and antipinholin ($S^{21}68_{IRS}$) proteins in a lipid bilayer. Using these distance restraints, the structural topology and conformational dynamics of $S^{21}68$ and $S^{21}68_{IRS}$ were refined using the simulated annealing software package Xplor-NIH. The results reveal distinct topological and conformational differences between active and inactive pinholin S^{21}. The data and the corresponding model clearly indicate that TMD2 of $S^{21}68$ remains incorporated in the lipid bilayer, while TMD1 lies on or near the surface of the lipid bilayer. However, the inactive form of antipinholin ($S^{21}68_{IRS}$) adopts a different conformation in which the TMDs have an approximately parallel alignment between TMD1 and TMD2, and both helices remain incorporated into the lipid bilayer. The data agree well with previous CW-EPR power saturation studies.[48,49]

EXPERIMENTAL METHODS

Peptide Synthesis, Purification, and Spin Labeling. All peptides were synthesized on an automated CEM Liberty Blue peptide synthesizer equipped with the Discovery Bio microwave system via optimized Fmoc-SPPS reported in previous studies.[48−50] After successful synthesis, the cleavage reaction ran for at least 3 h under optimized cocktail conditions to remove the resin and protecting groups from the peptide chain, followed by filtration, N_2 (g) evaporation, ether precipitation, and lyophilization.[48−50,70,71] The crude peptide was first purified by reverse-phase high-performance liquid chromatography (RP-HPLC) using a GE HPLC system coupled with a C4 (10 μm) preparative column (Vydac 214TP, 250 × 22 mm), as described previously.[48] The purified peptide was further purified using a C4 semipreparative column (Vydac 214TP, 250 × 10 mm). The lyophilized pure peptide was dissolved in dimethyl sulfoxide with a 10-fold excess of MTSL (1:5 M ratio for each spin label site) and stirred for 24 h in a dark environment to obtain the double

https://dx.doi.org/10.1021/acs.jpcb.0c09081
J. Phys. Chem. B 2020, 124, 11396−11405

spin-labeled peptide. The spin-labeled peptide was purified again with a C4 semipreparative column to remove free MTSL. After each purification, the purity of the target peptide was confirmed by MALDI-TOF MS. Spin labeling efficiency was calculated ~90−95% using CW-EPR spectroscopy.[50]

Peptide Incorporation into Proteoliposomes. For the DEER measurements, each spin-labeled pinholin or anti-pinholin peptide was incorporated into DMPC (1,2-dimyristoyl-*sn*-glycero-3-phosphocholine) proteoliposomes following the thin film method, as described previously.[48,50] A 20 mM HEPES (4-(2-hydroxyethyl)-1-piperazineethanesulfonic acid) buffer in D_2O (pH ~ 7.0) was used to rehydrate the thin film. D_2O was used instead of H_2O to improve the phase time memory of the EPR sample. The final concentrations of lipid and peptide were 50 mM and 50 μM, respectively, in the proteoliposome sample to get a 1000:1 lipid/peptide ratio unless specified. This ratio was chosen to minimize the effect of intermolecular interactions of pinholin, which has been shown to oligomerize in the penultimate step of the lysis mechanism.[35,43] A 30% (v/v) glycerol solution was added to each DEER sample as a cryoprotectant. Homogeneity and the size of the proteoliposomes samples were confirmed by using dynamic light scattering spectroscopy (ZETASIZER NANO Series; Malvern Instruments) at 25 °C in a disposable 40 μL microcuvette, and the average size (diameter) of the proteoliposome was ~200 nm.[48]

EPR Spectroscopic Measurements. All EPR experiments were conducted at the Ohio Advance EPR Laboratory of Miami University. All DEER samples were initially scanned with CW-EPR spectroscopy using an X-band (~9.34 GHz) Bruker EMX spectrometer equipped with an ER041xG microwave bridge and ER4119-HS cavity to confirm the quality of the samples. Experimental setups for CW-EPR spectroscopy were described previously.[48] The four-pulsed DEER experiments were conducted using a Bruker ELEXSYS E580 spectrometer with a SUPERQ-FT pulse Q-band system. The system first used a 10 W amplifier, but then was upgraded to a more powerful 300 W amplifier, with an EN5107D2 resonator. Approximately 70 μL of the sample was loaded into 3 mm quartz EPR tubes and flash frozen with liquid nitrogen just before loading into the resonator cavity. Experimental data were collected with 16-step phase cycling at a temperature of 80 K. An optimized four-pulsed sequence $[(\pi/2)_{\nu 1} - \tau_1 - (\pi)_{\nu 1} - t - (\pi)_{\nu 2} - (\tau_1 + \tau_2 - t) - (\pi)_{\nu 1} - \tau_2 - \text{echo}]$ was used for a dead time-free DEER experimental data collection.[67,72] The probe pulse width was 8/16 ns, and the pump $(\pi)_{\nu 2}$ pulse width was 24 ns. A 120 MHz frequency difference was used between the pump and probe pulses. In the upgraded instrumental setup, the pump $(\pi)_{\nu 2}$ pulse was a 70 ns frequency-swept chirp pulse spanning 85 MHz. The shot repetition time was 1000 μs with 100 shots/point. Data acquisition time was 2−3 μs, depending on the sample's phase memory time (T_2) and S/N ratio. Data acquisition was done overnight for signal averaging. DEER data analysis was conducted using the MATLAB DEER Analysis 2015 Program.[73,74] DEER distance distributions, $P(r)$, were obtained using Tikhonov regularization in the distance domain with the minimum distance constraint $P(r) > 0$ under DEER Analysis 2015.[73,74] Background correction was performed using a two-dimensional homogeneous model for proteoliposomes. The best fit of the time domain data was used for optimizing the regularization parameter in the L-curve.

Structure Refinement of the Active and Inactive Conformations of Pinholin S^{21} Using DEER Distance Restraints. The structural refinement of the active and inactive forms of pinholin S^{21} was carried out using an Xplor-NIH (version 2.46) simulated annealing protocol[75,76] in a similar manner to that described previously.[77−79] A starting structure was obtained by modeling the peptide standard α-helical dihedral angles ($\Phi = -57.0°$, $\psi = -47.0°$, and $\omega = 180.0°$) for the backbone of the TMDs of the active conformations of pinholin S^{21} using a *VEGA ZZ 3.0.5* simulation toolkit.[80] Positions 16, 17, 20, 24, 27, 38, 40, 44, and 46 along the active form of the pinholin S^{21} sequence were mutated to Cys, and MTSL side chains were attached with the Xplor-NIH addAtoms.py script using NIH-Xplor-2.46.[75,76] Experimental DEER data for five interlabel distances (16/46, 17/38, 20/44, 24/40, and 27/38) on the active version of pinholin were used to define restraints for an Xplor-NIH simulated annealing protocol for active pinholin. A starting structure was obtained by using the amino acid sequence of the inactive conformation of pinholin S^{21} on the template structure of the helix 3 and helix 4 (S3−S4) segments of KCNQ1-VSD (PDB ID: 5VMS) under Xplor-NIH using the Xplor-NIH addAtoms.py script. This template was used because the structural conformation was similar to that of the inactive antipinholin, based on an earlier study by Ry Young group.[32,37] Positions 8, 14, 15, 24, 27, 38, 40, and 53 along the inactive form of the pinholin S^{21} sequence were mutated to Cys, and MTSL side chains were attached with the Xplor-NIH addAtoms.py script. Experimental DEER data for five interlabel distances (8/53, 14/53, 15/53, 24/40, and 27/38) on the inactive version of pinholin were used to define restraints for an Xplor-NIH simulated annealing protocol for inactive pinholin. The allowable ranges used for interlabel distances were established through a series of preliminary simulated annealing molecular dynamics calculations in which these ranges were varied.[79] One hundred structures were generated using the Xplor-NIH simulated annealing routine with the Xplor-NIH_foldB.py script. The 10 lowest energy structures were further refined using a simulated annealing protocol using the Xplor-NIH refine_EEF.py script using the above-mentioned DEER distance restraints, using an implicit solvent model incorporated in the eefxPotTools module included in the refine_EEF.py script.[81,82] The membrane thickness of 25.4 Å (corresponding to that of the DMPC lipid) was used to model the DMPC lipid bilayer. A value of 0.85 was used to scale the dielectric screening, as suggested in the refine_EEF.py script. The simulated annealing procedure used 3500 K as the high temperature and 25 K as the cooling temperature, with temperature steps of 12.5 K. The eight lowest energy structures were kept with energies <−1824.46 kcal/mol for the active conformation of pinholin. Similarly, the eight lowest energy structures were kept with energies <107.60 kcal/mol for the inactive conformation of pinholin. These lowest energy structures were further validated against DEER distance restraints to make sure the spin label distances are within experimental errors.[82] Further analysis and visualization were done using the VMD-Xplor software.[83,84] The final structures were generated by replacing MTSL spin-labeled side chains with native side chains using the Xplor-NIH addAtoms.py script under Xplor-NIH, similar to a previously reported method.[79] Further details of the simulated annealing outputs are given in the Supporting Information (Tables S1 and S2).

https://dx.doi.org/10.1021/acs.jpcb.0c09081
J. Phys. Chem. B 2020, 124, 11396−11405

All MD simulations were run at the Miami Redhawk cluster computing facilities at Miami University.

RESULTS

Recently, we reported the structural dynamics and topology of $S^{21}68$ and $S^{21}68_{IRS}$ incorporated into DMPC proteoliposomes using SS-NMR spectroscopy, CW-EPR line-shape analysis, and power saturation techniques.[48−50,62] In this study, DEER spectroscopy is used to investigate the structural topology of active pinholin and inactive antipinholin and to demonstrate conformational differences between these two forms of pinholin S^{21}. Figure 1A,B shows the primary amino acid sequence for active pinholin ($S^{21}68$) and the inactive analog of antipinholin ($S^{21}68_{IRS}$) as a reference. Figure 1C,D is the tentative topology of the active and inactive conformations of pinholin S^{21}, respectively. To apply DEER spectroscopy to study the structural parameters of pinholin S^{21}, specific native amino acids were replaced with cysteine to introduce nitroxide spin labels at site-directed positions. In total, five dual spin-labeled full-length active pinholin ($S^{21}68$) and five dual spin-labeled inactive antipinholin ($S^{21}68_{IRS}$) peptides were studied. Spin label positions were judiciously selected to abate structural perturbation, based on published mutational analysis and our initial studies.[35,37,43,49]

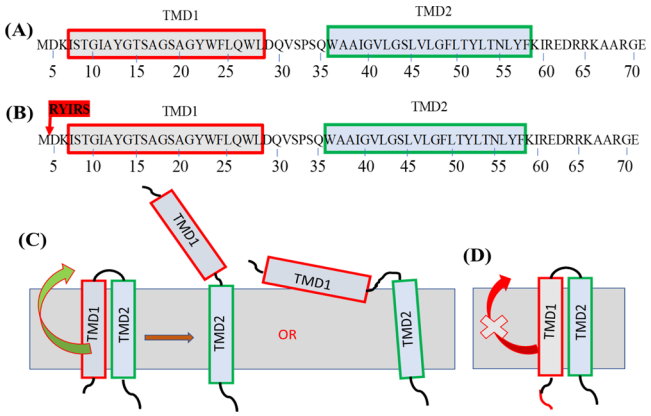

Figure 1. Primary sequence and tentative topology of active pinholin ($S^{21}68$) and inactive antipinholin ($S^{21}68_{IRS}$). TMD1 and TMD2 are indicated by red and green boxes, respectively. (A) The primary sequence of $S^{21}68$ and (B) the primary sequence of $S^{21}68_{IRS}$. "RYIRS" tag are incorporated between methionine and aspartate at the N-terminal. (C) Two possible orientations of $S^{21}68$, where TMD1 is completely externalized from the lipid bilayer or stays on the surface of the lipid−solvent interface. (D) The tentative topology of $S^{21}68_{IRS}$.

DEER Distance Measurement for the Active Conformation of Pinholin $S^{21}68$. The structural and functional biochemical literature on pinholin $S^{21}68$ suggests that TMD1 of pinholin $S^{21}68$ externalizes from the lipid bilayer, while TMD2 remains incorporated in the lipid bilayer to achieve the active conformation of pinholin $S^{21}68$.[31,32,37,43,48,62] However, there is no concrete experimental evidence to show that TMD1 remains in the periplasm after externalization and the relative orientation of TMD1 and TMD2. Based on Cys cross-linking and accessibility of disulfide bonds, Ry Young's lab proposed the complete externalization of TMD1 from the lipid bilayer.[33] However, recent biophysical studies have indicated a partial externalization of TMD1, which lies on the surface of the lipid bilayer to adapt a topology where TMD1 is almost perpendicular to TMD2, based on CW-EPR line-shape analysis, power saturation, and solid-state NMR experiments.[48,62] Both proposed conformations are shown in Figure 1C.

To investigate the relative orientation and distance between TMD1 and TMD2 of $S^{21}68$, DEER spectroscopy was used, in which one spin label was placed on TMD1 and another spin label on TMD2. The positions of the spin labels were judiciously selected based on the published literature data and our initial experimental results.[37,48] Spin pairs were designed to show the relative distance between TMD1 and TMD2, and positions of the spin labels as a pair are shown in Figure 2A. The extreme ends of N- and C-termini were avoided considering the fact that the distance distribution could fall outside the detection limit for membrane protein studies in a lipid bilayer because of the short phase memory time for DEER experiments.[85] Again, distances longer than 50 Å are sometimes suppressed by background correction and can generate artifact peaks at long distances for a data-trace length of 2 μs.[85] Multiple DEER spectra of $S^{21}68$ in DMPC proteoliposomes are shown in Figure 2B−F. The baseline-corrected time-domain traces (left) are shown with the corresponding distance probability distributions from Tikhonov regularization (right). Table 1 presents the final DEER distance summary obtained for $S^{21}68$ with the error limit of ±4 Å. The DEER distance data clearly demonstrate that the distances between two spin labels increases gradually when spin pairs move from the loop region to the terminus regions, which indicates that the N-terminus of TMD1 is further apart from the C-terminus of TMD2. The shortest distance observed was 24 Å for W27_A38, and the longest distance was 49 Å for S16_V46 (Table 1). These distance restraints were used for the structural model of active pinholin $S^{21}68$ using the simulated annealing software package Xplor-NIH for refinement.

DEER Distance Measurements for the Inactive Conformation of Antipinholin ($S^{21}68_{IRS}$). To investigate the structural conformation and the relative orientation and distance between TMD1 and TMD2 of $S^{21}68_{IRS}$, one spin label was placed on TMD1 and another on TMD2 of $S^{21}68_{IRS}$. Figure 3A shows the spin label positions on the structural model of $S^{21}68_{IRS}$. Spin label pairs were designed to minimize structural perturbations, based on previous studies in the literature.[37,48] This was critical for TMD1, which has a natural tendency to externalize, and certain single mutations can (e.g. G21Q) cause activation of antipinholin (implies externalization of TMD1), as reported by Pang et al.[37] The DEER data and corresponding distance probability distributions for each pair of spin labels on $S^{21}68_{IRS}$ are shown in Figure 3B−F.

The shortest distance was 23 Å for W27R1_A38R1 (close to the loop region), which remains within the experimental error for the rest of the parallel spin pair distances. The distance between terminal regions (S8R1_L53R1) was found to be 26 Å, which is unlikely if TMD1 is externalized and moves far from TMD2, like the active form of pinholin. Other distances were 25, 26, and 25 Å for F24R1_G40R1, T15R1_L53R1, and G14R1_L53R1, respectively. Table 2 presents the final DEER distance summary obtained for inactive antipinholin ($S^{21}68_{IRS}$). These distance restraints were used for the structural refinement of $S^{21}68_{IRS}$ using the simulated annealing software package Xplor-NIH.

Structural Model of $S^{21}68$ and $S^{21}68_{IRS}$ from MTSL DEER Distance Restraints. A structural model for the most probable structure of active pinholin ($S^{21}68$) and inactive

https://dx.doi.org/10.1021/acs.jpcb.0c09081
J. Phys. Chem. B 2020, 124, 11396−11405

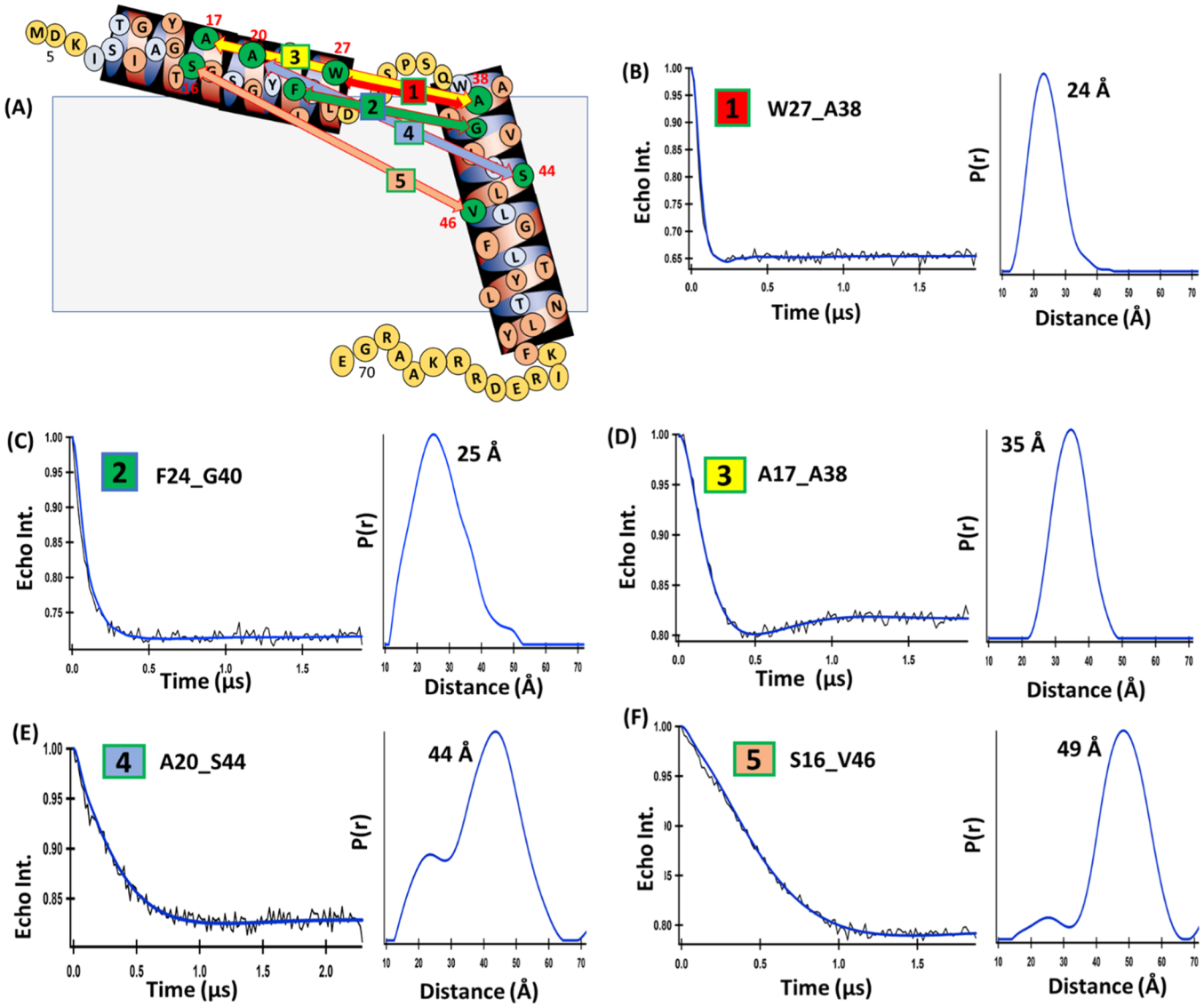

Figure 2. Q-band DEER data of active pinholin $S^{21}68$ in DMPC proteoliposomes. (A) Spin label positions in the structural model, and (B–E) the corresponding DEER distances with time-domain data.

Table 1. Summary of the Major Peak DEER Distance for the Active Conformation of $S^{21}68$

spin labels positions on $S^{21}68$	distance (±4 Å)
(1) W27R1_A38R1	24
(2) F24R1_G40R1	25
(3) A17R1_A38R1	35
(4) A20R1_S44R1	44
(5) S16R1_V46R1	49

antipinholin ($S^{21}68_{IRS}$) in DMPC proteoliposomes was obtained using the experimentally determined DEER distances coupled with the simulated annealing software package Xplor-NIH (version 2.46).[75,76] The DEER distance data obtained for five pairs of MTSL spin-labeled sites in proteoliposomes, independently for both $S^{21}68$ (Table 1) and $S^{21}68_{IRS}$ (Table 2), were converted into Xplor distance restraints and utilized in a simulated annealing protocol (see Experimental Methods). The MTSL DEER distance restraints were used to make the structure calculation procedure simpler within Xplor-NIH. Since MTSL is a widely used spin probe for EPR spectroscopic studies, the method of structure refinement used in this study can be widely applied to many other membrane proteins. A series of simulated annealing calculations were performed using distance-restraint uncertainties of ±4 Å, independently for both $S^{21}68$ and $S^{21}68_{IRS}$. Figure 4 displays the eight lowest energy structures from a family of 100 calculated structures of both $S^{21}68$ and $S^{21}68_{IRS}$ in proteoliposomes, obtained from the simulated annealing calculation using MTSL-derived distance restraints. These structures satisfied experimental DEER distances within experimental errors. To generate the final structures, the MTSL spin-labeled side chains were replaced by the native side chains with retention of the C_β position in the label. The output energies corresponding to eight minimum energy structures obtained from Xplor-NIH refinement are given in the Supporting Information (Tables S1 and S2).

DISCUSSION

Q-band DEER distance measurement coupled with simulated annealing molecular dynamics clearly demonstrates two different structural conformations and topology for active pinholin versus inactive antipinholin S^{21} with respect to the

https://dx.doi.org/10.1021/acs.jpcb.0c09081
J. Phys. Chem. B 2020, 124, 11396–11405

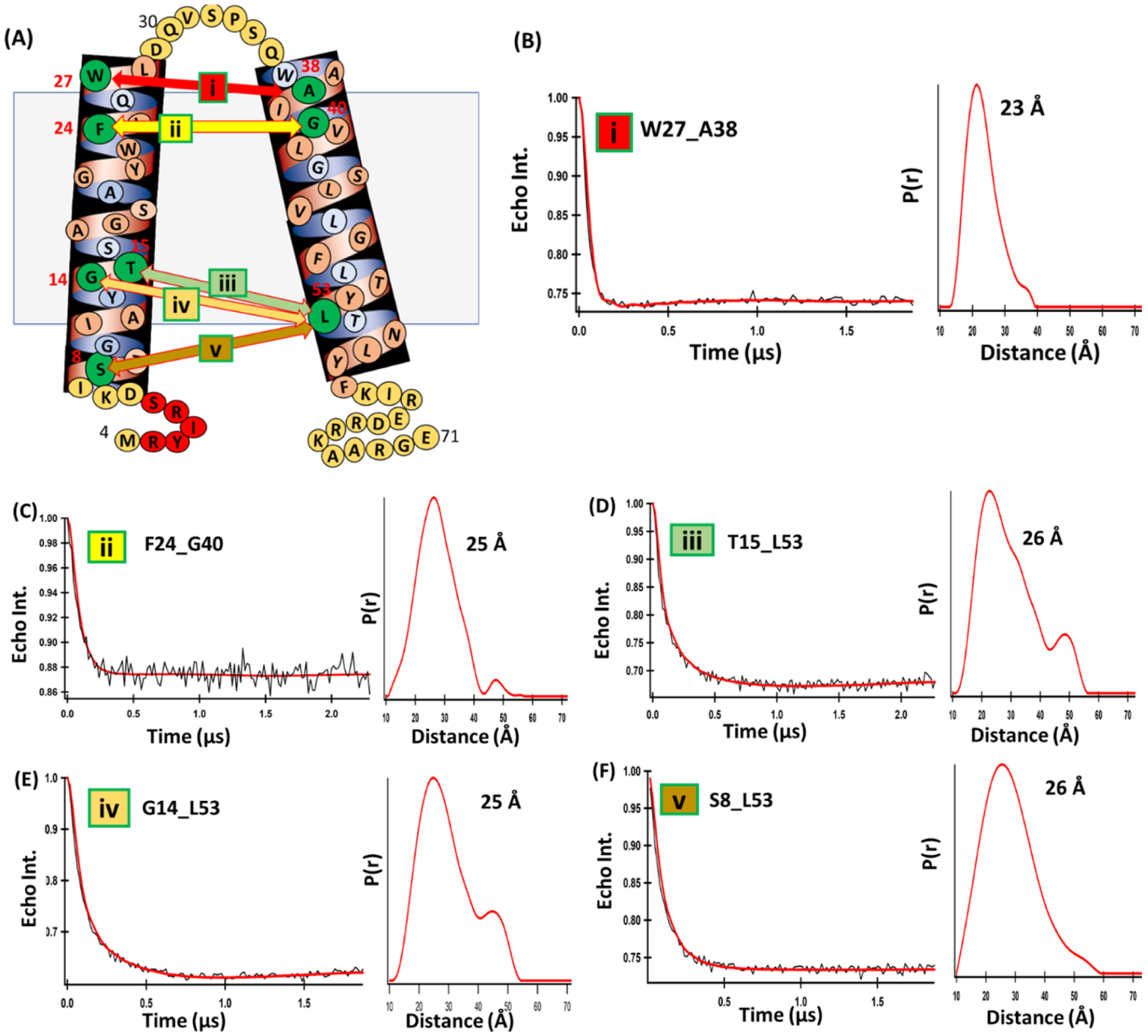

Figure 3. Q-band DEER data for inactive pinholin $S^{21}68_{IRS}$ in DMPC proteoliposomes. (A) Spin label positions are shown in the structural model, with (B–E) the corresponding DEER time-domain data and distance probability distributions.

Table 2. Summary of the Major Peak DEER Distance for the Inactive Conformation of $S^{21}68_{IRS}$

spin labels positions on $S^{21}68_{IRS}$	distance (±4 Å)
(i) W27R1_A38R1	23
(ii) F24R1_G40R1	25
(iii) T15R1_L53R1	26
(iv) G14R1_L53R1	25
(v) S8R1_L53R1	26

membrane bilayer. Distances between spin labels on TMD1 and TMD2 for inactive antipinholin clearly indicate that both helices remain in close proximity with a parallel conformation, maintaining an average distance of 23–26 Å. Our previous studies using CW-EPR, power saturation, and solid-state NMR indicated that both helices most likely remain in the lipid bilayer for inactive antipinholin, which was consistent with the model proposed by the Young group.[32,62] The structural model

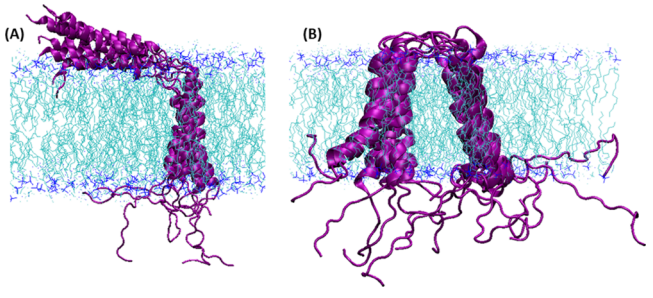

Figure 4. Structural models of active pinholin and inactive antipinholin incorporating MTSL DEER distance restraint data using an Xplor-NIH simulated annealing molecular dynamics protocol. Overlay of the ribbon representation of the eight structures with the lowest energy obtained from restrained simulated annealing calculations using the amino acids of $S^{21}68$ (A) and $S^{21}68_{IRS}$ (B). Images were created using the VMD-Xplor program.[83]

https://dx.doi.org/10.1021/acs.jpcb.0c09081
J. Phys. Chem. B 2020, 124, 11396–11405

obtained using DEER distance restrains and the simulated annealing molecular dynamics simulation (Figure 4B) is consistent with the previous biophysical EPR and biochemical data.[32,49]

For the active form of pinholin S^{21}, DEER distances between spin labels on TMD1 and TMD2 clearly indicate that the N-terminal of TMD1 is moving away from the C-terminal of TMD2 and support the notion that TMD1 externalizes from the lipid bilayer.[32,48,62] Considering our previous CW-EPR power saturation studies and the proposed model by Young's lab, it was confirmed that TMD2 remains inside the lipid bilayer, which implies that TMD1 moves away from TMD2 and is externalized from the lipid bilayer.[32,33,48,62] However, it was not certain what the orientation of TMD1 is relative to TMD2 after externalization, and two probable orientations were proposed in the literature, as shown in Figure 1C. The distance between S16R1 and V46R1 was found to be 49 Å, which would be a much longer distance if TMD1 completely externalized from the lipid bilayer, as shown in Figure 1C. This clearly supports the orientation where TMD1 lies on the membrane surface and is perpendicular with TMD2 instead of being completely externalized. Although, we are not completely excluding the probability of complete externalization, considering the fact that a dynamic protein like pinholin can adopt multiple conformations, where the majority of the population remains in the perpendicular orientation on the surface and some population remains in completely externalized orientations. This may be one of the possible reasons for the broadening of the DEER distribution for most of the DEER data obtained in this study. Longer DEER distances above 50 Å can get suppressed for membrane proteins incorporated into a lipid bilayer because of the short data acquisition time and background subtraction, which becomes undetectable or nontrivial for a very small population.[85] At the same time, shorter distance populations around 25 Å probably arose from a small population of active pinholin in which TMD1 did not externalize from the lipid bilayer and was oriented parallel with TMD2 and/or intermolecular distances between adjacent TMD2−TMD2 because of the natural propensity of oligomerization for active pinholin in the presence of a lipid bilayer. Oligomerization was minimized in the study by conducting the experiments at a low (1000:1) lipid/peptide ratio. The DEER structural models obtained for both active pinholin and inactive antipinholin are consistent with our earlier studies and biological experiments conducted by the Ry Young group.[32,37,48,49,62] However, this study was performed in the presence of DMPC proteoliposomes. Further studies are needed with different lipid bilayers to generalize the structural model in different membrane environments.

CONCLUSIONS

This study reported structural models and conformations of both the active pinholin and inactive antipinholin forms of the phage Φ21 lytic proteins in a lipid bilayer, using DEER spectroscopy coupled with the simulated annealing molecular dynamics (MD). DEER distance distributions and the derived structural model using the simulated annealing MD simulation demonstrated clear conformational differences between the two forms of the pinholin S^{21} protein. Furthermore, this study reported refined structural models of these two proteins and resolved existing conflict in structural models of active pinholin in the field. The structural model of S^{21} presented in this study will be useful for understanding the structural and functional relationship of pinholin S^{21} as well as other holin systems using biophysical techniques. This study will help researchers apply these powerful EPR spectroscopic approaches to investigate conformational changes in more complicated membrane protein systems and hence will move the structural biology field forward.

ASSOCIATED CONTENT

Supporting Information

The Supporting Information is available free of charge at https://pubs.acs.org/doi/10.1021/acs.jpcb.0c09081.

Minimum energy associated with the refined structures of active and inactive pinholin obtained from the simulated annealing molecular dynamics simulation (PDF)

AUTHOR INFORMATION

Corresponding Author

Gary A. Lorigan − *Department of Chemistry and Biochemistry, Miami University, Oxford, Ohio 45056, United States;* orcid.org/0000-0002-2395-3459; Phone: (513) 529-2813; Email: gary.lorigan@miamioh.edu; Fax: (513) 529-5715

Authors

Tanbir Ahammad − *Department of Chemistry and Biochemistry, Miami University, Oxford, Ohio 45056, United States*

Daniel L. Drew, Jr. − *Department of Chemistry and Biochemistry, Miami University, Oxford, Ohio 45056, United States*

Indra D. Sahu − *Department of Chemistry and Biochemistry, Miami University, Oxford, Ohio 45056, United States; Natural Science Division, Campbellsville University, Campbellsville, Kentucky 42718, United States*

Rasal H. Khan − *Department of Chemistry and Biochemistry, Miami University, Oxford, Ohio 45056, United States*

Brandon J. Butcher − *Department of Chemistry and Biochemistry, Miami University, Oxford, Ohio 45056, United States*

Rachel A. Serafin − *Department of Chemistry and Biochemistry, Miami University, Oxford, Ohio 45056, United States*

Alberto P. Galende − *Natural Science Division, Campbellsville University, Campbellsville, Kentucky 42718, United States*

Robert M. McCarrick − *Department of Chemistry and Biochemistry, Miami University, Oxford, Ohio 45056, United States*

Complete contact information is available at: https://pubs.acs.org/10.1021/acs.jpcb.0c09081

Notes

The authors declare no competing financial interest.

ACKNOWLEDGMENTS

We are grateful to the members of the Ry Young group at Texas A&M University for their experimental suggestions. We would also like to appreciate Dr. Jens Mueller, the Facility Manager, Redhawk Cluster Miami University, for assistance with the computational work. This work was generously

supported by the NIGMS/NIH Maximizing Investigator's Research Award (MIRA) R35 GM126935, the NSF CHE-1807131 grant, the NSF (MRI-1725502) grant, the Ohio Board of Regents, and Miami University. G.A.L. would also like to acknowledge support from the John W. Steube Professorship.

REFERENCES

(1) Saier, M. H., Jr.; Reddy, B. L. Holins in bacteria, eukaryotes, and archaea: Multifunctional xenologues with potential biotechnological and biomedical applications. *J. Bacteriol.* **2015**, *197*, 7−17.
(2) Yoong, P.; Schuch, R.; Nelson, D.; Fischetti, V. A. Identification of a broadly active phage lytic enzyme with lethal activity against antibiotic-resistant Enterococcus faecalis and Enterococcus faecium. *J. Bacteriol.* **2004**, *186*, 4808−4812.
(3) Fischetti, V. A. Bacteriophage lytic enzymes: novel anti-infectives. *Trends Microbiol.* **2005**, *13*, 491−496.
(4) Bernhardt, T. G.; Wang, I.-N.; Struck, D. K.; Young, R. Breaking free: "Protein antibiotics" and phage lysis. *Res. Microbiol.* **2002**, *153*, 493−501.
(5) Shi, Y.; Li, N.; Yan, Y.; Wang, H.; Li, Y.; Lu, C.; Sun, J. Combined antibacterial activity of phage lytic proteins holin and lysin from streptococcus suis bacteriophage SMP. *Curr. Microbiol.* **2012**, *65*, 28−34.
(6) Alvi, I. A.; Asif, M.; Tabassum, R.; Aslam, R.; Abbas, Z.; Rehman, S. U. RLP, A bacteriophage of the family Podoviridae, rescues mice from bacteremia caused by multi-drug-resistant Pseudomonas aeruginosa. *Arch. Virol.* **2020**, *165*, 1289.
(7) Cof fey, B.; Mills, S.; Coffey, A.; McAuliffe, O.; Ross, R. P. Phage and their lysins as biocontrol agents for food safety applications. *Annu. Rev. Food Sci. Technol.* **2010**, *1*, 449−468.
(8) Callewaert, L.; Walmagh, M.; Michiels, C. W.; Lavigne, R. Food applications of bacterial cell wall hydrolases. *Curr. Opin. Biotechnol.* **2011**, *22*, 164−171.
(9) Loessner, M. J. Bacteriophage endolysins - current state of research and applications. *Curr. Opin. Microbiol.* **2005**, *8*, 480−487.
(10) Agu, C. A.; Klein, R.; Schwab, S.; König-Schuster, M.; Kodajova, P.; Ausserlechner, M.; Binishofer, B.; Bläsi, U.; Salmons, B.; Günzburg, W. H.; et al. The cytotoxic activity of the bacteriophage lambda-holin protein reduces tumour growth rates in mammary cancer cell xenograft models. *J. Gene Med.* **2006**, *8*, 229−241.
(11) Agu, C. A.; Klein, R.; Lengler, J.; Schilcher, F.; Gregor, W.; Peterbauer, T.; Bläsi, U.; Salmons, B.; Günzburg, W. H.; Hohenadl, C. Bacteriophage-encoded toxins: the lambda-holin protein causes caspase-independent non-apoptotic cell death of eukaryotic cells. *Cell. Microbiol.* **2007**, *9*, 1753−1765.
(12) Brandtner, E. M.; Kodajova, P.; Hlavaty, J.; Jandl, G.; Tabotta, W.; Salmons, B.; Günzburg, W. H.; Hohenadl, C. Reconstituting retroviral (ReCon) vectors facilitating delivery of cytotoxic genes in cancer gene therapy approaches. *J. Gene Med.* **2008**, *10*, 113−122.
(13) Lu, N.; Sun, Y.; Wang, Q.; Qiu, Y.; Chen, Z.; Wen, Y.; Wang, S.; Song, Y. Cloning and characterization of endolysin and holin from Streptomyces avermitilis bacteriophage phiSASD1 as potential novel antibiotic candidates. *Int. J. Biol. Macromol.* **2020**, *147*, 980−989.
(14) Young, R. Bacteriophage holins: Deadly diversity. *J. Mol. Microbiol. Biotechnol.* **2002**, *4*, 21−36.
(15) Young, R. Phage Lysis: Three steps, three choices, one outcome. *J. Microbial.* **2014**, *52*, 243−258.
(16) Berry, J.; Rajaure, M.; Pang, T.; Young, R. The spanin complex is essential for lambda lysis. *J. Bacteriol.* **2012**, *194*, 5667−5674.
(17) Berry, J.; Summer, E. J.; Struck, D. K.; Young, R. The final step in the phage infection cycle: the Rz and Rz1 lysis proteins link the inner and outer membranes. *Mol. Microbiol.* **2008**, *70*, 341−351.
(18) Graschopf, A.; Bläsi, U. Functional assembly of the lambda S holin requires periplasmic localization of its N-terminus. *Arch. Microbiol.* **1999**, *172*, 31−39.
(19) Zhang, N.; Young, R. Complementation and characterization of the nested Rz and Rz1 reading frames in the genome of bacteriophage λ. *Mol. Gen. Genet.* **1999**, *262*, 659−667.
(20) Cahill, J.; Young, R. Phage lysis: multiple genes for multiple barriers. *Adv. Virus Res.* **2019**, *103*, 33−70.
(21) Chang, C. Y.; Nam, K.; Young, R. S-gene expression and the timing of lysis by bacteriophage-lambda. *J. Bacteriol.* **1995**, *177*, 3283−3294.
(22) R, Y.; IN, W. Phage Lysis. *The bacteriophages*, 2nd ed.; Oxford University Press: Oxford, 2006; p 104−126.
(23) Young, R. Phage lysis: do we have the hole story yet? *Curr. Opin. Microbiol.* **2013**, *16*, 790−797.
(24) Young, R. Bacteriophage lysis - mechanism and regulation. *Microbial. Rev.* **1992**, *56*, 430−481.
(25) Bläsi, U.; Young, R. Two beginnings for a single purpose: The dual-start holins in the regulation of phage lysis. *Mol. Microbiol.* **1996**, *21*, 675−682.
(26) Savva, C. G.; Dewey, J. S.; Deaton, J.; White, R. L.; Struck, D. K.; Holzenburg, A.; Young, R. The holin of bacteriophage lambda forms rings with large diameter. *Mol. Microbiol.* **2008**, *69*, 784−793.
(27) Savva, C. G.; Dewey, J. S.; Moussa, S. H.; To, K. H.; Holzenburg, A.; Young, R. Stable micron-scale holes are a general feature of canonical holins. *Mol. Microbiol.* **2014**, *91*, 57−65.
(28) To, K. H.; Young, R. Probing the structure of the S105 hole. *J. Bacteriol.* **2014**, *196*, 3683−3689.
(29) White, R.; Chiba, S.; Pang, T.; Dewey, J. S.; Savva, C. G.; Holzenburg, A.; Pogliano, K.; Young, R. Holin triggering in real time. *Proc. Natl. Acad. Sci. U.S.A.* **2011**, *108*, 798−803.
(30) Wang, I.-N.; Deaton, J.; Young, R. Sizing the Holin Lesion with an Endolysin-β-Galactosidase Fusion. *J. Bacteriol.* **2003**, *185*, 779−787.
(31) Park, T.; Struck, D. K.; Dankenbring, C. A.; Young, R. The pinholin of lambdoid phage 21: Control of lysis by membrane depolarization. *J. Bacteriol.* **2007**, *189*, 9135−9139.
(32) Pang, T.; Savva, C. G.; Fleming, K. G.; Struck, D. K.; Young, R. Structure of the lethal phage pinhole. *Proc. Natl. Acad. Sci. U.S.A.* **2009**, *106*, 18966−18971.
(33) Park, T.; Struck, D. K.; Deaton, J. F.; Young, R. Topological dynamics of holins in programmed bacterial lysis. *Proc. Natl. Acad. Sci. U.S.A.* **2006**, *103*, 19713−19718.
(34) Barenboim, M.; Chang, C.-Y.; dib Hajj, F.; Young, R. Characterization of the dual start motif of a class II holin gene. *Mol. Microbiol.* **1999**, *32*, 715−727.
(35) Pang, T.; Park, T.; Young, R. Mapping the pinhole formation pathway of S21. *Mol. Microbiol.* **2010**, *78*, 710−719.
(36) Wang, I.-N.; Smith, D. L.; Young, R. Holins: The protein clocks of bacteriophage infections. *Annu. Rev. Microbiol.* **2000**, *54*, 799−825.
(37) Pang, T.; Park, T.; Young, R. Mutational analysis of the S21 pinholin. *Mol. Microbiol.* **2010**, *76*, 68−77.
(38) Columbus, L.; Hubbell, W. L. A new spin on protein dynamics. *Trends Biochem. Sci.* **2002**, *27*, 288−295.
(39) Volkman, B. F.; Lipson, D.; Wemmer, D. E.; Kern, D. Two-state allosteric behavior in a single-domain signaling protein. *Science* **2001**, *291*, 2429−2433.
(40) Mulder, F. A. A.; Mittermaier, A.; Hon, B.; Dahlquist, F. W.; Kay, L. E. Studying excited states of proteins by NMR spectroscopy. *Nat. Struct. Biol.* **2001**, *8*, 932−935.
(41) Rozovsky, S.; Jogl, G.; Tong, L.; McDermott, A. E. Solution-state NMR investigations of triosephosphate isomerase active site loop motion: Ligand release in relation to active site loop dynamics. *J. Mol. Biol.* **2001**, *310*, 271−280.
(42) Ishima, R.; Freedberg, D. I.; Wang, Y.-X.; Louis, J. M.; Torchia, D. A. Flap opening and dimer-interface flexibility in the free and inhibitor-bound HIV protease, and their implications for function. *Structure* **1999**, *7*, 1047−1055.
(43) Pang, T.; Fleming, T. C.; Pogliano, K.; Young, R. Visualization of pinholin lesions in vivo. *Proc. Natl. Acad. Sci. U.S.A.* **2013**, *110*, E2054−E2063.

https://dx.doi.org/10.1021/acs.jpcb.0c09081
J. Phys. Chem. B 2020, 124, 11396−11405

(44) Torres, J.; Stevens, T. J.; Samsó, M. Membrane proteins: The "Wild West" of structural biology. *Trends Biochem. Sci.* **2003**, *28*, 137−144.
(45) Wüthrich, K. NMR studies of structure and function of biological macromolecules (Nobel Lecture). *J. Biomol. NMR* **2003**, *27*, 13−39.
(46) Schiemann, O.; Prisner, T. F. Long-range distance determinations in biomacromolecules by EPR spectroscopy. *Q. Rev. Biophys.* **2007**, *40*, 1−53.
(47) Acharya, K. R.; Lloyd, M. D. The advantages and limitations of protein crystal structures. *Trends Pharmacol. Sci.* **2005**, *26*, 10−14.
(48) Ahammad, T.; Drew, D. L.; Sahu, I. D.; Serafin, R. A.; Clowes, K. R.; Lorigan, G. A. Continuous wave electron paramagnetic resonance spectroscopy reveals the structural topology and dynamic properties of active pinholin S(21)68 in a lipid bilayer. *J. Phys. Chem. B* **2019**, *123*, 8048−8056.
(49) Ahammad, T.; Drew, D. L.; Khan, R. H.; Sahu, I. D.; Faul, E.; Li, T.; Lorigan, G. A. Structural dynamics and topology of the inactive form of S21 holin in a lipid bilayer using continuous-wave electron paramagnetic resonance spectroscopy. *J. Phys. Chem. B* **2020**, *124*, 5370−5379.
(50) Drew, D. L., Jr.; Ahammad, T.; Serafin, R. A.; Butcher, B. J.; Clowes, K. R.; Drake, Z.; Sahu, I. D.; McCarrick, R. M.; Lorigan, G. A. Solid phase synthesis and spectroscopic characterization of the active and inactive forms of bacteriophage S21 pinholin protein. *Anal. Biochem.* **2019**, *567*, 14−20.
(51) Sahu, I. D.; McCarrick, R. M.; Lorigan, G. A. Use of Electron paramagnetic resonance to solve biochemical problems. *Biochemistry* **2013**, *52*, 5967−5984.
(52) Altenbach, C.; Froncisz, W.; Hemker, R.; McHaourab, H.; Hubbell, W. L. Accessibility of nitroxide side chains: Absolute Heisenberg exchange rates from power saturation EPR. *Biophys. J.* **2005**, *89*, 2103−2112.
(53) Pyka, J.; Ilnicki, J.; Altenbach, C.; Hubbell, W. L.; Froncisz, W. Accessibility and dynamics of nitroxide side chains in T4 lysozyme measured by saturation recovery EPR. *Biophys. J.* **2005**, *89*, 2059−2068.
(54) Hubbell, W. L.; Altenbach, C. Investigation of structure and dynamics in membrane-proteins using site-directed spin-labeling. *Curr. Opin. Struct. Biol.* **1994**, *4*, 566−573.
(55) Hubbell, W. L.; McHaourab, H. S.; Altenbach, C.; Lietzow, M. A. Watching proteins move using site-directed spin labeling. *Structure* **1996**, *4*, 779−783.
(56) Hubbell, W. L.; Gross, A.; Langen, R.; Lietzow, M. A. Recent advances in site-directed spin labeling of proteins. *Curr. Opin. Struct. Biol.* **1998**, *8*, 649−656.
(57) Hubbell, W. L.; Cafiso, D. S.; Altenbach, C. Identifying conformational changes with site-directed spin labeling. *Nat. Struct. Biol.* **2000**, *7*, 735−739.
(58) Bates, I. R.; Boggs, J. M.; Feix, J. B.; Harauz, G. Membrane-anchoring and charge effects in the interaction of myelin basic protein with lipid bilayers studied by site-directed spin labeling. *J. Biol. Chem.* **2003**, *278*, 29041−29047.
(59) Klug, C. S.; Feix, J. B. Methods and applications of site-directed spin Labeling EPR Spectroscopy. *Biophysical Tools for Biologists: Vol 1 in Vitro Techniques*; Academic Press, 2008; Vol. *84*, pp 617−658.
(60) Altenbach, C.; Marti, T.; Khorana, H.; Hubbell, W. Transmembrane protein-structure - spin labeling of bacteriorhodopsin mutants. *Science* **1990**, *248*, 1088−1092.
(61) Altenbach, C.; Greenhalgh, D. A.; Khorana, H. G.; Hubbell, W. L. A collision gradient-method to determine the immersion depth of nitroxides in lipid bilayers - application to spin-labeled mutants of bacteriorhodopsin. *Proc. Natl. Acad. Sci. U.S.A.* **1994**, *91*, 1667−1671.
(62) Drew, D. L., Jr.; Butcher, B.; Sahu, I. D.; Ahammad, T.; Dixit, G.; Lorigan, G. A. Active S2168 and inactive S21IRS pinholin interact differently with the lipid bilayer: A 31P and 2H solid state NMR study. *Biochim. Biophys. Acta, Biomembr.* **2020**, *1862*, 183257.
(63) Sahu, I. D.; Lorigan, G. A. Biophysical EPR studies applied to membrane proteins. *J. Phys. Chem. Biophys.* **2015**, *5*, 188.
(64) Jeschke, G.; Polyhach, Y. Distance measurements on spin-labelled biomacromolecules by pulsed electron paramagnetic resonance. *Phys. Chem. Chem. Phys.* **2007**, *9*, 1895−1910.
(65) Borbat, P. P.; McHaourab, H. S.; Freed, J. H. Protein structure determination using long-distance constraints from double-quantum coherence ESR: Study of T4 lysozyme. *J. Am. Chem. Soc.* **2002**, *124*, 5304−5314.
(66) Vicente, E. F.; Sahu, I. D.; Costa-Filho, A. J.; Chilli, E. M.; Lorigan, G. A. Conformational changes of the HsDHODH N-terminal microdomain via DEER Spectroscopy. *J. Phys. Chem. B* **2015**, *119*, 8693−8697.
(67) Jeschke, G. DEER Distance Measurements on Proteins. *Annu. Rev. Phys. Chem.* **2012**, *63*, 419−446.
(68) Sahu, I. D.; McCarrick, R. M.; Troxel, K. R.; Zhang, R.; Smith, H. J.; Dunagan, M. M.; Swartz, M. S.; Rajan, P. V.; Kroncke, B. M.; Sanders, C. R.; Lorigan, G. A. DEER EPR measurements for membrane protein structures via bifunctional spin labels and lipodisq nanoparticles. *Biochemistry* **2013**, *52*, 6627−6632.
(69) Sahu, I. D.; Lorigan, G. A. Site-Directed spin labeling EPR for studying membrane proteins. *BioMed Res. Int.* **2018**, *2018*, 3248289.
(70) Bottorf, L.; Sahu, I. D.; McCarrick, R. M.; Lorigan, G. A. Utilization of C-13-labeled amino acids to probe the alpha-helical local secondary structure of a membrane peptide using electron spin echo envelope modulation (ESEEM) spectroscopy. *Biochim. Biophys. Acta, Biomembr.* **2018**, *1860*, 1447−1451.
(71) Mayo, D. J.; Sahu, I. D.; Lorigan, G. A. Assessing topology and surface orientation of an antimicrobial peptide magainin 2 using mechanically aligned bilayers and electron paramagnetic resonance spectroscopy. *Chem. Phys. Lipids* **2018**, *213*, 124−130.
(72) Pannier, M.; Veit, S.; Godt, A.; Jeschke, G.; Spiess, H. W. Dead-time free measurement of dipole-dipole interactions between electron spins. *J. Magn. Reson.* **2000**, *142*, 331−340.
(73) Jeschke, G.; Chechik, V.; Ionita, P.; Godt, A.; Zimmermann, H.; Banham, J.; Timmel, C. R.; Hilger, D.; Jung, H. DeerAnalysis2006 - a comprehensive software package for analyzing pulsed ELDOR data. *Appl. Magn. Reson.* **2006**, *30*, 473−498.
(74) Chiang, Y.-W.; Borbat, P. P.; Freed, J. H. The determination of pair distance distributions by pulsed ESR using Tikhonov regularization. *J. Magn. Reson.* **2005**, *172*, 279−295.
(75) Schwieters, C. D.; Kuszewski, J. J.; Tjandra, N.; Marius Clore, G. The Xplor-NIH NMR molecular structure determination package. *J. Magn. Reson.* **2003**, *160*, 65−73.
(76) Schwieters, C.; Kuszewski, J.; Mariusclore, G. Using Xplor-NIH for NMR molecular structure determination. *Prog. Nucl. Magn. Reson. Spectrosc.* **2006**, *48*, 47−62.
(77) Mokdad, A.; Herrick, D. Z.; Kahn, A. K.; Andrews, E.; Kim, M.; Cafiso, D. S. Ligand-Induced structural changes in the escherichia coli ferric citrate transporter reveal modes for regulating protein-protein interactions. *J. Mol. Biol.* **2012**, *423*, 818−830.
(78) Herrick, D. Z.; Kuo, W.; Huang, H.; Schwieters, C. D.; Ellena, J. F.; Cafiso, D. S. Solution and membrane-bound conformations of the tandem C2A and C2B domains of synaptotagmin 1: Evidence for bilayer bridging. *J. Mol. Biol.* **2009**, *390*, 913−923.
(79) Jao, C. C.; Hegde, B. G.; Chen, J.; Haworth, I. S.; Langen, R. Structure of membrane-bound alpha-synuclein from site-directed spin labeling and computational refinement. *Proc. Natl. Acad. Sci. U.S.A.* **2008**, *105*, 19666−19671.
(80) Pedretti, A.; Villa, L.; Vistoli, G. VEGA - An open platform to develop chemo-bio-informatics applications, using plug-in architecture and script programming. *J. Comput.-Aided Mol. Des.* **2004**, *18*, 167−173.
(81) Schwieters, C. D.; Bermejo, G. A.; Clore, G. M. Xplor-NIH for molecular structure determination from NMR and other data sources. *Protein Sci.* **2018**, *27*, 26−40.
(82) Sahu, I. D.; Kroncke, B. M.; Zhang, R.; Dunagan, M. M.; Smith, H. J.; Craig, A.; McCarrick, R. M.; Sanders, C. R.; Lorigan, G. A. Structural investigation of the transmembrane domain of KCNE1 in proteoliposomes. *Biochemistry* **2014**, *53*, 6392−6401.

https://dx.doi.org/10.1021/acs.jpcb.0c09081
J. Phys. Chem. B 2020, 124, 11396−11405

(83) Schwieters, C. D.; Clore, G. M. The VMD-XPLOR visualization package for NMR structure refinement. *J. Magn. Reson.* **2001**, *149*, 239−244.
(84) Humphrey, W.; Dalke, A.; Schulten, K. VMD: Visual molecular dynamics. *J. Mol. Graphics Modell.* **1996**, *14*, 33−38.
(85) Jeschke, G. The contribution of modern EPR to structural biology. *Emerging Top. Life Sci.* **2018**, *2*, 9−18.

https://dx.doi.org/10.1021/acs.jpcb.0c09081
J. Phys. Chem. B 2020, 124, 11396−11405